Application of Highlight Removal and Multivariate Image Analysis to Color Measurement of Flotation Bubble Images

Chunhua Yang, Canhui Xu, Weihua Gui, Kaijun Zhou

School of Information Science and Engineering, Central South University, Hunan 410083, People's Republic of China

Received 4 June 2008; revised 11 July 2009; accepted 13 July 2009

ABSTRACT: Machine vision based analysis provides a novel technology for froth flotation monitoring. Froth images collected are characterized by fully occupied bubbles with different size and shape under various illuminations. Convex bubbles lead to the formation of white spots that seriously affect froth color measurement. In this article, specular highlights are detected and preprocessed so as to estimate underlying color of white spots region. Because of the fact that color information is believed to be related to flotation performance, therefore, after the application of highlight inpainting, multivariate image analysis is proposed to extract color features, which are further related to mineral grades by a orthogonal least square regression model. The established relationship provides a promising empirical model to predict mineral grade, which is a significant indicator for flotation performance. Experimental results show that, when compared with traditional methods, the proposed algorithm can achieve a robust color measurement and predict mineral concentration effectively. © 2009 Wiley Periodicals, Inc. Int J Imaging Syst Technol, 19, 316–322, 2009; Published online in Wiley InterScience (www.interscience.wiley.com). DOI 10.1002/ima.20208

Key words: flotation; highlight inpainting; machine vision; multivariate image analysis; total variation

I. INTRODUCTION

Flotation is an indispensable technology to effectively utilize the low-graded ore resources. It aims to separate valuable minerals from useless materials or other minerals through complex physiochemical processes. By the addition of chemicals and mixture of air, valuable minerals are made hydrophobic to attach to the air bubbles, which rise up to the froth layer on the top of slurry, where the upgraded valuable minerals are collected. Flotation is a multivariate process influenced by many factors, such as reagent doses of chemicals, air flow, feed ore grade, grinded particle size, etc. The control and modeling of flotation processes are challenging due to the inherently chaotic nature of the underlying microscopic phenomena. At present, the control of flotation process depends heavily on human operators' various experience by viewing the visual appearance of the froth. Lack of online reliable sensors and subjective problems caused by operator's limitation pose additional difficulties. Recent developments in digital image processing provide new opportunities to gain a better understanding of the industrial flotation process (Moolman et al., 1996). As a soft measurement in mineral flotation process, image processing sensors can provide quantitative measures of froth characteristics, objective description of froth appearance, and nonintrusive real time monitoring with little maintenance.

It is widely known that the froth characteristics such as the color, bubble structure, morphology, and speed are closely related, in a quantitative way, to mineral grade (concentrations), process status and recovery, respectively. Numerous reported literatures are devoted to the extraction of froth image features like texture color (Bartolacci et al., 2006), bubble size (Chunhua et al., 2009), froth speed (Holtham and Nguyen, 2002), and bubble load (Ventura-Medina and Cilliers, 2000). Color and texture information is believed to strongly associate with mineral concentration. Early work applied the image gray intensity and a measure of the relative red on 35 mm film captured static froth images, derived from the RGB (red, green, blue) color space (Hargrave and Hall, 1997). Others explored froth color discriminability in various color space like RGB, HSV (hue, saturation, value), and HSI (hue, saturation, intensity) (Bonifazi et al., 2001). Duchesne proposed the application of multivariate image analysis (MIA) to predict the concentrate grade and achieved good prediction results (Duchesne et al., 2003). Bartolacci reported several image processing methodologies to analyze froth color and texture, including the famous MIA, gray-level co-occurrence matrix (GLCM), and wavelet transform analysis (WTA) methods (Bartolacci et al., 2006). It is claimed that MIA method captures the froth variation relatively better than WTA method. An improved version of MIA called multiresolutional MIA (MR-MIA II) was developed to extract relevant color information and detect clear windows and black holes in the froth images (Liu et al., 2005). A more recent research tried to design models and controller based on MR-MIA analysis (Liu and MacGregor, 2008).

Correspondence to: Canhui Xu; e-mail: xucanhui2005@126.com

Grant sponsors: This article is supported by the Key Program of National Natural Science of China under Grant No. 60634020, the National Natural Science Foundation of China under Grant No. 60874069, and the Specialized Research Fund for the Doctoral Program of Higher Education of China under Grant No. 200805331104.

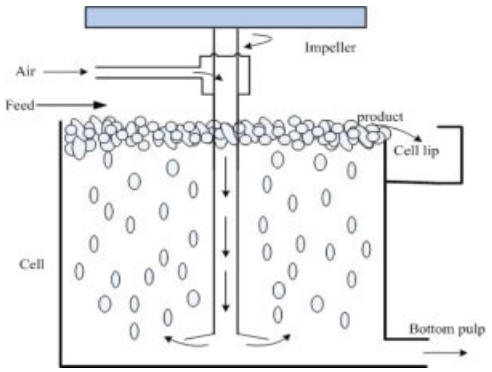

Figure 1. Scheme of individual flotation cell. [Color figure can be viewed in the online issue, which is available at www.interscience.wiley.com.]

Bubble images collected from industry field show that large amount of highlight region (white spots) appears on the top of bubbles, which not only affects accurate color feature extraction, but also deteriorates the segmentation results due to strong edges caused by spotlights. It is a new perspective to remove the highlight artifacts, which can help the reconstruction of underlying color of white spots and benefit the segmentation performance by overcoming oversegmentation effects caused by uneven illumination. A newly reported research on the robustness of color measurement emphasizes that the effect of lighting on froth color measurement is un-negligible, and a LAB color space was proposed to measure the luminosity and chromaticity (Reddick et al., 2009).

This work aims to characterize mineral flotation froth through digital image processing techniques and predict mineral concentration based on robust color measurement. An effective preprocessing scheme is carried out on each collected bubble image to remove specular highlights and estimate accurate color of bubble. The correlation between the intensities of image spectra is explored by using MIA. Based on the principle component loading coefficients of RGB images, an orthogonal least square (OLS) regression model is built for the purpose of predicting the mineral grade. Industrial case study reveals the efficiency and reliability of the proposed methodology.

Next section reviews the mechanism of the flotation process as well as the introduction of experimental set-up. Section III introduces highlight detection and removal using total variation inpainting. In Section IV, color spectral information is studied and multivariate statistical analysis is proposed to extract loading coefficients of color variance. Section V presents the experimental results and discussion. Conclusion is provided in the last section.

II. FLOTATION PROCESS AND EXPERIMENTAL SET-UP

The process of froth flotation entails crushing and grinding of the raw ore to a fine size. The fine particles are mixed with water and the slurry (pulp) is fed in the flotation cells, which agitate the mixture and introduce air continuously to form a large number of bubbles as shown in Figure 1.

Experiments are carried out on industrial scale in a bauxite flotation plant of China. The test set-up consists of RGB cameras with 49 mm lens placed $\sim$110 cm above the surface of flotation froth layer. Froth image sequences, derived from videos captured at the rate of 7.5 frames/s, are collected from individual flotation cell with a volume of 16 m^3. The window size of each image in a cell is 12 $\times$ 9 cm^2. It should be noticed that how to choose the specific position of surface for the collection is crucial to capture high-quality images. Some researchers chose the position for installing camera near the cell lip focusing on the measurement of velocity. For froth with its size varying from 1 mm to 20 mm, we explored other possible positions to acquire qualified images which are significant for the subsequent processing like bubble structure and color extraction. On the opposite side of the cell lip, a position near the impeller seems to be a better choice for two reasons: the use of froth discharge paddles near the cell lip will agitate bubbles around (Moolman et al., 1996), so positions can be chosen far away from cell lips to avoid much bubble collision and keep more mineral particles attached on itself; on the other hand, bubbles are relatively ''fresh'' and newly rising with less fracture caused by the pressing among bubbles. Ambient light is prevented from reflecting in by iron cover on the cell top. The camera is mounted above the target cell, with video output transmitted by optic fiber to the digital computer, shown in Figure 2.

As discovered, froth images collected from industry field show that: (1) a froth image is fully occupied by bubbles, in normal cases, with no void space or background region between bubbles; (2) the illumination on bubble surface is uneven; (3) each bubble has a convex shape which leads to the appearance of white spots, generally on the top if the incident ray is from the vertical direction of froth layer.

Human operators usually check the feed ore grade (input) in rougher cells, tail grade (output) in scavenger cells, and cleaning grade (product) in cleaning cells (Fig. 3). The operators take control actions mainly based on feedback of minerals grade measured by X-ray fluorescence (XRF) analyzer or titration. The sampling (10–20 min) and titration of grade measurement (2–3 h) take long time to give prompt feedback for process monitoring and control. To estimate the mineral grade and get the whole picture of the flotation process, it is agreed that bubble images should be acquired from rougher, scavenging, and cleaning cells by installing the cameras in positions as Figure 3 shows.

III. HIGHLIGHT REMOVAL

When recording natural scene images, highlights due to specular reflection are often taken into consideration, especially in the case that the underlying color or texture is of importance for image analyses. The highlight problem becomes even serious as the light source and camera position are along the identical direction, in this work, which is vertical to top froth phase. As observed, the collected bubble images are found to have various uneven white highlight spots, which results in the occlusion of underlying color

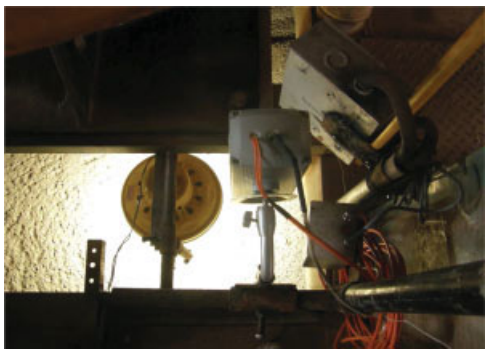

Figure 2. Image acquisition hardware configuration. [Color figure can be viewed in the online issue, which is available at www.interscience.wiley.com.]

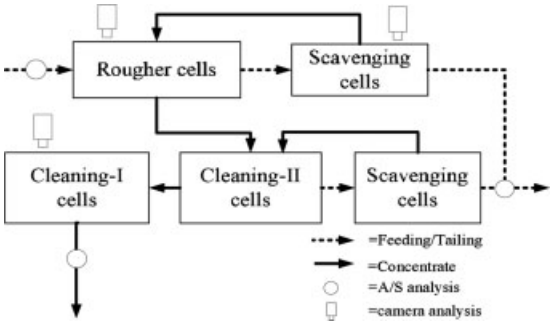

Figure 3. Flowchart of flotation circuit and installing positions of RGB cameras.

information. Although various literatures consider color measurement as a crucial feature to be connected with the mineral grade, a few considered the artifacts caused by highlights, which is also known as color constancy problem in computer vision field.

Assuming that bubble images are not overimposed when collected, highlights can be detected simply in HSV color space by thresholds on saturation and value (Hue component is much insensitive to light variances). The obtained highlight region is further processed by region growing method.

On the basis of Shafer's dichromatic reflection model (Shafer, 1985) to remove highlight for a single-image case (Klinker, 1990), Klinker proved that every pixel from dielectric materials can be described as a linear combination of diffuse color and highlight color (Klinker et al., 1987). And all the diffuse and highlight pixels form linear clusters in a T-shape. Highlight can be removed by projecting highlight colors onto the diffuse vector to compute underlying diffuse color. Highlight cluster, however, is often skewed due to surface roughness and image geometry. Reliable estimation of real color for natural images can hardly be achieved (Norvak and Shafer, 1992).

From another perspective, highlight removal has a close connection with image inpainting. The objective of inpainting is to fill the missing and damaged region by propagating the surrounding information and structure (Bertalmio et al., 2000; Barcelos and Batista, 2008). Consider that our images have large amount of highlight regions on the top of bubbles to be filled in. Total variation (TV) inpainting model proposed by Chan and Shen (2002) can give smooth interpolation. The rationale behind is that the inpainting can be achieved by minimizing the following regularity function over the highlight region D using adjacent pixels in region E (Fig. 4),

$$R(u) = \int_{E\cup D} r|\nabla u| dxdy, \tag{1}$$

under the denoizing constraint on E

$$\frac{1}{\text{Area}(E)} \int_E |u - u^0|^2 dxdy = \sigma^2, \tag{2}$$

where u is missing image value to be inpainted, r is an appropriate real function which is nonnegative for nonnegative inputs, u^0 is contaminated by homogeneous Gaussian white noise, and σ is the standard deviation of white noise. Using the Lagrange multiplier, constrained variational problem (1)–(2) is solved by minimizing

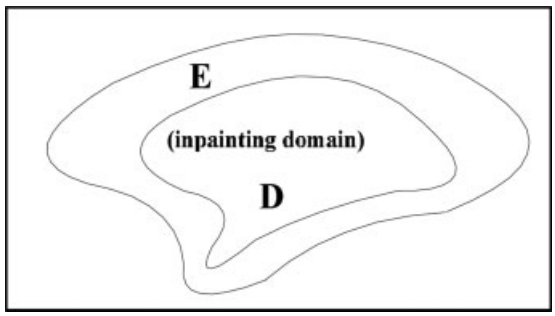

Figure 4. Inpainting domain and extended domain.

$$J_\lambda(u) = \int_{E\cup D} |\nabla u| dxdy + \frac{\lambda}{2} \int_E |u - u^0|^2 dxdy, \tag{3}$$

where λ is the Lagrange multiplier.

The Euler-Lagrange equation for the energy functional J_λ is

$$-\nabla \cdot \left(\frac{\nabla u}{|\nabla u|} \right) + \lambda_e (u - u^0) = 0, \tag{4}$$

where

$$\lambda_e = \begin{cases} \lambda, (x,y) \in E \\ 0, (x,y) \in D \end{cases}.$$

The numerical scheme for the TV inpainting model is designed. As shown in Figure 5, at a given target pixel O, let $\Lambda = \{E, N, W, S\}$ denote its four adjacent pixels and $\{e, n, w, s\}$ denote the corresponding four midway points, which are not digital image pixels. Let $v = (v^1, v^2) = \frac{\nabla u}{|\nabla u|}$. Then the divergence is discretized by central differencing:

$$\nabla \cdot v = \frac{\partial v^1}{\partial x} + \frac{\partial v^2}{\partial y} \approx \frac{v_e^1 - v_w^1}{h} + \frac{v_n^2 - v_s^2}{h}, \tag{5}$$

where the grid size h is taken to be 1. Take the midpoint e as an example, approximation at midway point is calculated by

$$v_e^1 = \frac{1}{\nabla u_e} \left[\frac{\partial u}{\partial x} \right]_e \approx \frac{1}{|\nabla u_e|} \frac{u_E - u_O}{h}, \tag{6}$$

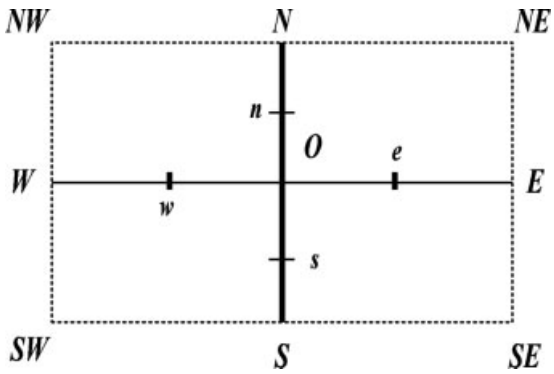

Figure 5. A target pixel O and its neighbors.

$$|\nabla u_e| \approx \frac{1}{h}\sqrt{(u_E - u_O)^2 + [(u_{NE} + u_N - u_S - u_{SE})/4]^2}, \quad (7)$$

Therefore, (4) is discretized to

$$\sum_{P\in\Lambda} \frac{1}{|\nabla u_p|}(u_O - u_P) + \lambda_e(O)(u_O - u_O^0) = 0, \quad (8)$$

Define

$$w_P = \frac{1}{|\nabla u_p|}, P \in \Lambda, \quad (9)$$

$$h_{OP} = \frac{w_P}{\sum_{P\in\Lambda} w_p + \lambda_e(O)}, \quad (10)$$

$$h_{OO} = \frac{\lambda_e(O)}{\sum_{P\in\Lambda} w_p + \lambda_e(O)}. \quad (11)$$

Then (8) becomes

$$u_O = \sum\nolimits_{P\in\Lambda} h_{OP} u_P + h_{OO} u_O^0. \quad (12)$$

Adopting the Gauss-Jacobi iteration scheme, at each step n, u^{n-1} can be updated to u^n by

$$u_O^{(n)} = \sum\nolimits_{P\in\Lambda} h_{OP}^{(n-1)} u_P^{(n-1)} + h_{OO}^{(n-1)} u_O^{(n-1)}, \quad (13)$$

As $h_{OP} + h_{OO} = 1$, formula (12) is stable.

According to (13), the highlight regions can be filled by executing the following steps:

1. Read bubble image I and detect its corresponding highlight regions H_0 as the mask template;
2. For each pixel (x, y) in I falling into the mask domain H_0, execute steps 3–5;
3. Calculate the midway points' first order derivative v_e^1 and gradient absolute value $|\nabla u_e|$;
4. For pixel (x, y) inside the mask domain H_0, set $\lambda_e(O)$ to be 0;
5. Calculate h_{OP} and h_{OO} to update pixels in region H_0, and save the new pixel value to original bubble image;
6. If the difference between the update image and original image is smaller than a set threshold, recursively carry out steps 2–5, otherwise, exit.

IV. MULTIVARIATE STATISTICAL ANALYSIS

The concept of the MIA was first proposed by Esbensen and Geladi (1989). Duchesne applied MIA for prediction of the concentrate grade (Duchesne, 2003). Later, Bartolacci reported the application of MIA to image analysis of copper flotation froth (Bartolacci et al., 2006). It is a multivariate statistical method considering the entire froth image as the model input and extracting the color variance for the prediction of mineral grade.

Assume that the RGB image X can be expressed as linear combination of N distinct features θ_i, where $1 \le i \le N$

$$X = \sum_{i=1}^{N} \phi_i(X) \cdot \theta_i. \quad (14)$$

The features span a relatively low-dimensional subspace where all the observed input can be projected onto by using the principal components of the data correlation matrix as features.

A RGB color image is viewed as a three-way array of data, with two spatial dimensions being geometrical coordinates and the third dimension being the spectral coordinate corresponding to the light intensity recorded by the camera in the red, green, and blue channels. Generally, the RGB image X ($M \times N \times 3$) is unfolded into a two-way matrix $\overline{X}$. The columns of $\overline{X}$ correspond to the red, green, and blue color intensities for each pixel of image, whereas each row corresponds to a particular pixel of the image. PCA is then applied to matrix $\overline{X}$:

$$\bar{X} = \sum_{i=1}^{k} T_i \cdot p_i^T + E, \quad (15)$$

where K is the number of principal components (PCs), T_i is the score vectors (score images), and p_i is the loading vectors, $i = 1,\ldots, K$. Matrix E is the decomposition residual array and is zero when all PCs are used ($K = 3$ in this case). The decomposition of each unfolded image yields a series of loading vectors p_i, which are linear combination of the original RGB intensities explaining most of the color variations across the image and can be used directly as color features. Each loading vector p_i contains three weights corresponding to red, green, and blue colors. The first two PCs are considered in this work. For each loading vector p_i, the first two vectors p_1 and p_2 are chosen to represent color variations because they explained more than 99% of variance in color intensities. Thus, six features are extracted to represent color variations.

To visually demonstrate the decomposition of MIA, color features are extracted for two typical rougher bubble images sized 600 $\times$ 800 pixels. Note that in Figure 6, the first loading vector p_1 gives almost equal weights to three color channels, a weighted average of all three R, G, and B channels and its corresponding score image is similar to the gray-scale version of a RGB image. The second loading vector p_2 shows a great contrast between intensity value of red and blue. For these two different types of froth images, it is not difficult to identify the color variance by human visual system and tell difference between one with darkish, round bubbles and the other with reddish, uneven sized bubbles. These two types froth image correspond to different mineral separation performance, which is directly reflected by mineral grade. In practice, human operators often use the discriminative color as heuristic knowledge to manipulate the operational variables.

The loading vectors p_i of image a and b are

$$p_{ai} = \begin{bmatrix} 0.6094 & 0.6341 \\ 0.5665 & 0.0716 \\ 0.5546 & -0.7699 \end{bmatrix}, \quad p_{bi} = \begin{bmatrix} 0.7355 & 0.5274 \\ 0.5458 & -0.0893 \\ 0.4014 & -0.8449 \end{bmatrix}$$

respectively, which are plotted in Figure 6.

After applying the MIA to the images and extracting loading coefficients, a regression model is built to establish relationship between color features extracted from images and minerals grade so as to predict the A/S ratio, which was usually measured by XRF analyzer and calculated by $Q_{A1_2O_3}/Q_{SiO_2}$, where $Q_{A1_2O_3}$ is the quality

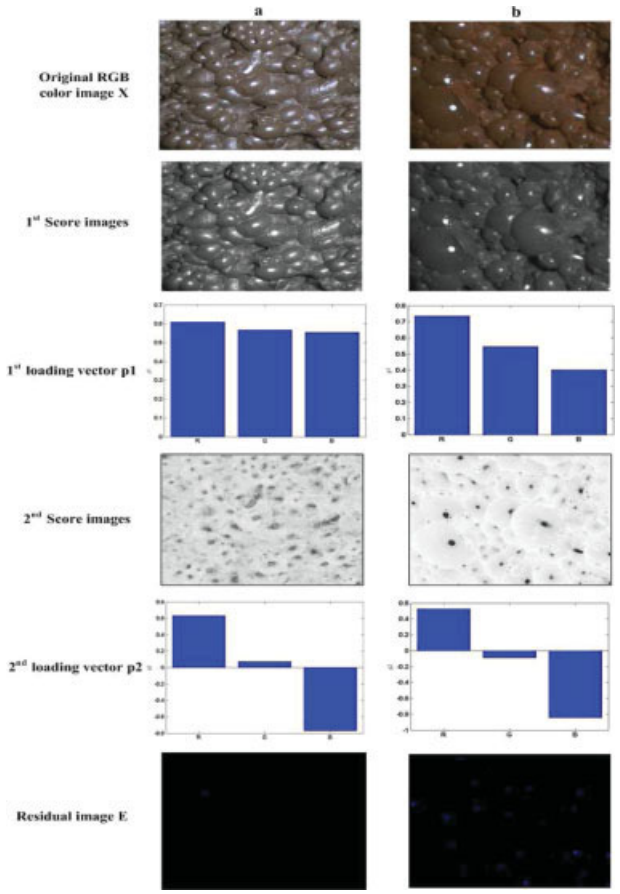

Figure 6. An illustration of MIA decomposition of typical RGB froth image from rougher cell. [Color figure can be viewed in the online issue, which is available at www.interscience.wiley.com.]

of Al_2O_3 and Q_{SiO_2} is the quality of SiO_2. For each image, color features are stored row-wise in a regression matrix X ($n \times l$), where n is the number of images used to build the model and l is the number of color features used in the model. Y ($n \times 1$) corresponds to mineral A/S grade measurement of froth images. OLS regression was used. It is a latent variable method defined as:

$$Y = XW + F, \tag{16}$$

where X contains the loading vectors, loading matrix W defines the relationship between the two spaces X and Y. F contains the regression error.

V. CASE STUDY RESULTS AND DISCUSSION

Experiments covering a large range of operating conditions are carried out on three different cells including rougher, scavenger, and cleaner. Online videos and froth images with the size of 600 × 800 pixels are recorded by RGB cameras over the flotation cells in a flotation industry field of China since the year 2008. Assumptions are made that videos collected from rougher cell can reflect the status of feed ore; videos from scavenger provide the information of tail grade; and videos from cleaner can gave the situation of product grade. The bubble videos are collected under the same condition (resolution, angle, light condition, position, view scale, etc.) 24 h a day. All the images are online collected RGB color images, with 256 intensity levels in each channel. Pulp samples are collected by our group members at exact same time of video recording and its corresponding A/S ratios are measured by XRF analyzer, which takes 20 min to accomplish the sample analysis. In practice, human operators measured the A/S ratios in the way of chemical titration which takes more than 2 h.

After acquiring qualified bubble videos, each image is preprocessed for the purpose of highlight removal. To obtain a robust measurement of color, each frame is first enhanced by denoizing to eliminate noise pixels with high intensities affecting highlight detection and then processed with HSV thresholds. The threshold region is further dilated by region growing method and then used as a mask image. Most of the top highlight regions can be reconstructed by total variation inpainting approach proposed in Section II. As shown in the first row of Figure 7, the inpainted visual results are promising. After processing the highlight reflection and recovering the underlying color, MIA approach has been carried out to extract color features. Different from the loading vectors calculated without highlight inpainting, the loading vectors p_i of image a and b are transferred into:

$$p_{ai} = \begin{bmatrix} 0.6367 & 0.6582 \\ 0.5698 & 0.0507 \\ 0.5195 & -0.7511 \end{bmatrix}, \quad p_{bi} = \begin{bmatrix} 0.7574 & 0.5263 \\ 0.5453 & -0.1844 \\ 0.3591 & -0.8301 \end{bmatrix}.$$

In this study, it is found that red color is generally dominant in the original RGB bubble images compared with other colors, and the loading vector of red channel in the corresponding 1st and 2nd loading plots often has a big positive value. Especially, the loading value of inpainted red channel is usually higher than the one without inpainting processing. MIA with highlight inpainting preprocessing can capture the color variance in a more accurate way. This also explains the relative redness proposed by Hargrave (Hargrave

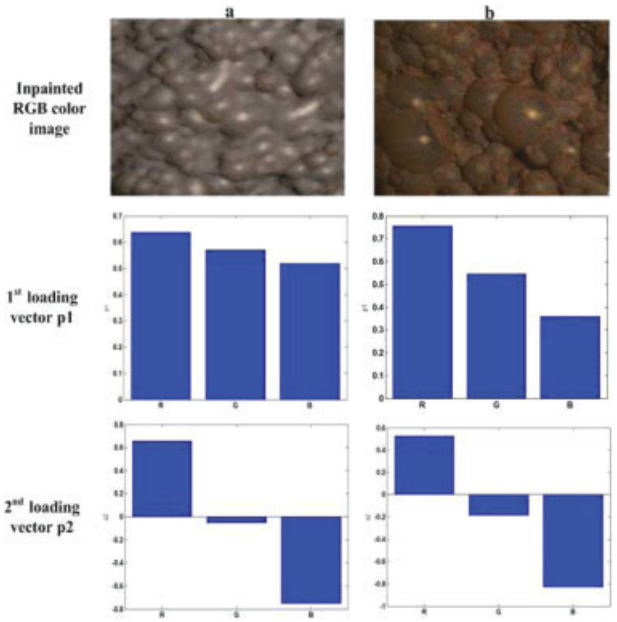

Figure 7. Two typical reconstructed bubble images using total variation inpainting (first row) and corresponding loading vectors. [Color figure can be viewed in the online issue, which is available at www.interscience.wiley.com.]

Table I. Prediction performance of the enhanced MIA empirical regression model in factory field.

Sample Time	Observed A/S	Predicted A/S	Error
2008.09.05.09	1.5800	1.5888	0.0088
2008.09.05.16	1.6615	1.6661	0.0064
2008.09.06.14	1.6869	1.7312	0.0443
2008.09.07.08	1.6167	1.7292	0.1125
2008.09.07.09	1.5926	1.5871	0.0055
2008.09.07.15	2.0764	2.0756	0.0008
2008.09.07.16	2.4238	2.5487	0.1249
2008.09.28.16	1.5875	1.60	0.0125

and Hall, 1997)) can relatively captures the discriminative color features well between froth images than regular RGB or HSV space, and used as a feature to classify the froth images and identify the bubble health status. MIA or its variations can outperform the relative redness for a sound description of color variance. It was also found that loading vectors were better color descriptors than means and standard deviations of RGB channel intensities.

Take rougher as an example, experiment covering a large range of operating conditions is performed to reflect the influence of feed ore. It is mentioned earlier that online videos are collected under the same resolution, angle, light condition, position, view scale, etc. Sixteen training video samples are from September 10 to 12, 2008, whereas eight testing videos are listed in Table I. Loading vectors for training video images are extracted to build OLS regression model. By using the obtained empirical regression model, mineral concentration of flotation pulp can be predicted when given testing dataset loading vectors.

To illustrate the clustering of the color feature, scatter plots of principal components are used to display the features in 2D spaces. Each point with coordinate (x, y) represents the first row of loading vector p_i of each video image. Points having similar color variations will fall into the identical region of the scatter plot. Thus, specific region in the scatter plot corresponding to a certain class of images can be identified. As shown in Figure 8a, the loading vector scatter plot of 80 images collected on September 10, 2008, is displayed by 80 asterisks. Sixty plus signs show the scatter plot of 60 images on September 11, 2008. Twenty squares represent the scatter plot of 20 images on September 12, 2008. From each video, 10 image frames are selected from each video recorded once an hour. At each time point, A/S grade is measured by XRF analyzer, which is denoted by the figure near each black circle. The sampling time of eight testing videos is listed in Table I. It also presents the prediction performance of the OLS regression. The 45° line in Figure 8b illustrates the correlation between predicted A/S and measured A/S ratios. Two dotted lines define the predictions falling within $\pm\sigma$ of grade analysis standard deviations, which show that the prediction results are within allowed prediction bias. The OLS regression model can capture the froth variations very well.

As shown, the prediction results are fascinating. However, there are situations when the workpoint is shifted or the operational balance is changed because of the feeding ore variety. Take videos from September 4, 2008, as an example, the scatter plot of loading vectors calculated is shown in Figure 8c. The ideal region of score plot has shifted accordingly, which demands further elaborate research to be done.

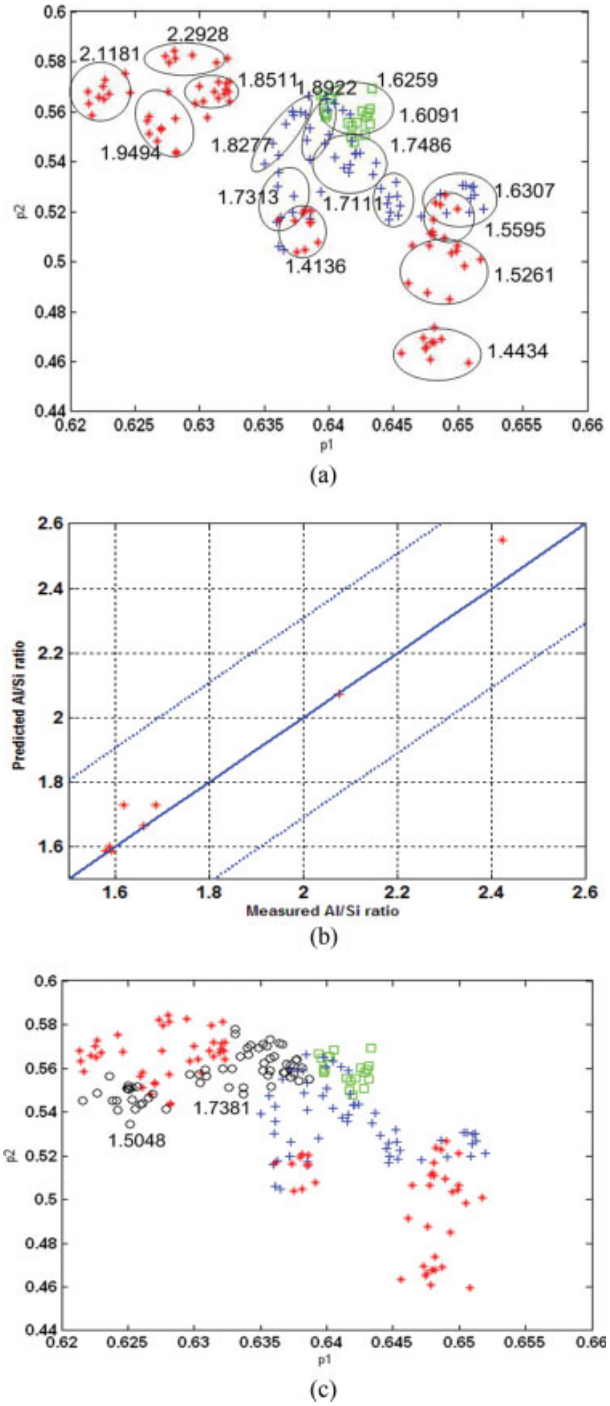

Figure 8. Scatter plots of extracted loading coefficients and mineral grade prediction results of OLS regression. (a) Scatter plots of all the images in training database. Black circles include 10 image frames from one video, and the figure beside corresponds to A/S ratio related to this video sample. Each marker represents the scatter plot of each RGB image, and marker with different shapes indicate images are from different dates. (b) Prediction of grade for A/S (measured versus predicted A/S grade). (c) Scatter plot of new loading coefficients for videos from September 4, 2008, and corresponding measured A/S ratio. [Color figure can be viewed in the online issue, which is available at www.interscience.wiley.com.]

VI. CONCLUSIONS

Based on the fact that color information is closely related to mineral grades according to human operators' heuristic knowledge, the issue of exploring correlation between the froth color variance and mineral concentration is investigated. Considering the white spot artifacts on bubble, total variation based highlight inpainting scheme is applied to enhance bubble images and reconstruct the underlying intensities for a robust color measurement. MIA is then applied to extract color features. An OLS regression model is utilized to predict mineral grade, which are of great economy importance for mineral industry. As shown, the results are promising when the workpoint is stable. The established relationship provides an empirical model to predict mineral concentration for industry process monitor and control. When compared with the MIA method, the enhanced bubble images are more robust to light variances.

REFERENCES

C.A.Z. Barcelos and M. Aurélio Batista, Image restoration using digital inpainting and noise removal, Image Vis Comput 25 (2008), 61–69.

G. Bartolacci, P. Pelletier Jr., J. Tessier Jr., C. Duchensene, P.-A. Bosse, and J. Fournier, Application of numerical image analysis to process diagnosis and physical parameter measurement in mineral processes. I. Flotation control based on froth textural characteristics, Miner Eng 19 (2006), 734–747.

M. Bertalmio, G. Sapiro, and V. Caselles, and C. Ballester, Image inpainting, Proceedings of SIGGRAPH, New Orleans, Louisiana, USA, July 23–28, 2000, pp. 417–424.

G. Bonifazi, S. Serranti, F. Volpe, and R. Zuco, Characterization of flotation froth structure and color by machine vision, Comput Geosci 27 (2001), 1111–1117.

T. Chan and J. Shen, Mathematical models for local nontexture inpainting, SIAM J Appl Math 62 (2002), 1019–1043.

C. Yang, C. Xu, X. Mou, and K. Zhou, Bubble size estimation using interfacial morphological information for mineral flotation process monitoring, Trans Nonferrous Metals Soc China 19(3) (2009), 694–699.

C. Duchesne, A. Bouajila, G. Bartolacci, P. Pelletier, Y. Breau, J. Fournier, and D. Girard, Application of multivariate image analysis (MIA) to predict concentrate grade in froth flotation processes, Proceedings of the 35th annual CMP meeting, Ottawa (Ontario), January 21–23, 2003, pp. 511–526.

K. Esbensen and P. Geladi, Strategy of multivariate image analysis (MIA), Chemometr Intell Lab Syst 7 (1989), 67–86.

J.M. Hargrave and S.T. Hall, Diagnosis of concentrate grade and mass flowrate in tin flotation from colour and surface texture analysis, Miner Eng 10 (1997), 613–621.

P.N. Holtham and K.K. Nguyen, On-line analysis of froth surface in coal and mineral flotation using JKFrothCam, Int J Miner Process 64 (2002), 163–180.

G.J. Klinker, A physical approach to color image understanding, Int J Comput Vis 4(1) (1990), 7–38.

G.J. Klinker, S.A. Shafer, and T. Kanade, Using a color reflection model to separate highlights from object color, ICCV, London, UK, 1987, pp. 145–150.

J.J. Liu and J.F. MacGregor, Froth-based modeling and control of flotation processes, Miner Eng 21(9) (2008), 642–651.

J.J. Liu, J.F. MacGregor, C. Duchesne, and G. Bartolacci, Flotation froth monitoring using multiresolutional multivariate image analysis, Miner Eng 18 (2005), 65–76.

D.W. Moolman, J.J. Eksteen, C. Aldrich, and J.S.J. van Deventer, The significance of flotation froth appearance for machine vision control, Int J Miner Process 48 (1996), 135–158.

J.F. Reddick, A.H. Hesketh, S.H. Morar, and D.J. Bradshaw, An evaluation of factors affecting the robustness of colour measurement and its potential to predict the grade of flotation concentrate, Miner Eng 22(1) (2009), 64–69.

S. Shafer, Using color to separate reflection components, Color Res Appl 10 (1985), 210–218.

E. Ventura-Medina and J.J. Cilliers, Calculation of the specific surface area in flotation, Miner Eng 13 (2000), 265–275.

C.L. Norvak and S.A. Shafer, Anatomy of a color histogram, Proceedings of IEEE Computer Vision and Pattern Recognition, June 15–18, 1992, pp. 259–268.